ACS APPLIED MATERIALS & INTERFACES

Research Article

www.acsami.org

Effective Solid Electrolyte Based on Benzothiazolium for Dye-Sensitized Solar Cells

Lu Han,[‡] Ye Feng Wang,*[,†,§] and Jing Hui Zeng[‡,§]

[†]School of Chemistry & Chemical Engineering, [‡]School of Materials Science and Engineering, and [§]Shaanxi Provincial Key Laboratory of Macromolecular Science, Chang'an Campus, Shaanxi Normal University, Xi'an 710620, China

Supporting Information

ABSTRACT: Thiaozole/benzothiaozole-based dicationic conductors were synthesized and applied as solid-state electrolyte in dye-sensitized solar cells (DSSCs). X-ray diffraction, scanning electron microscopy, thermal gravimetric analysis, steady-state voltammogram, photocurrent intensity−photovoltage test, and electrochemical impedance spectroscopy are used to characterize the materials and the mechanism of the cell performance. Compared to the traditional monocationic crystals, the dicationic crystals have a larger size and can provide more opportunities to fine-tune their physical/chemical properties. As a consequence, this solid-state electrolyte-based DSSC achieved photoelectric conversion efficiency of 7.90% under full air-mass (AM 1.5) sunlight (100 mW·cm^{-2}).

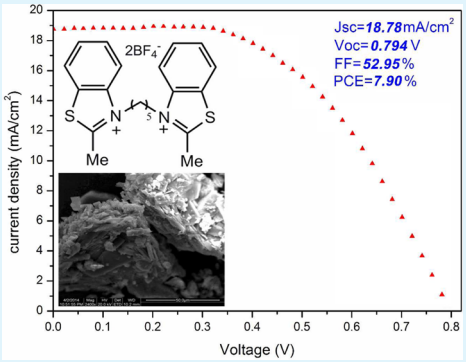

KEYWORDS: *electrolyte, dicationic, benzothiazolium,ion-conductor, ss-DSSCs*

INTRODUCTION

Electrolyte is one of the key components in dye-sensitized solar cell (DSSC) due to its function in charge-transfer and dye regeneration.[1] In a typical DSSC running cycle, electrons are generated upon photon excitation, then injected into the conduction band of semiconductors for photoanode, and transported to the outer circuit. Oxidized dye molecules are left behind and are reduced by the redox couple in the electrolyte. Subsequently, the oxidized redox couple diffuses into the counterelectrode for recovering.[2] Electrolyte is crucial in this cycle; its properties have great influence on the photo-conversion efficiency and stability of the device.[3] Although the photoelectric conversion efficiency of DSSC based on the liquid electrolyte has been achieved over 12%,[1,4] the volatility and leakage of liquid solvent in cells are prohibitive for outdoor application of DSSC in view of the need for robust encapsulation.[5] For this reason, there have been considerable efforts to replace the liquid electrolytes with solid-state counterparts to accelerate the future industrial production.[6,7]

Ionic conductors are promising candidates among the solid-state electrolyte materials for application in solid-state lithium batteries[8] and solid-state photovoltaic devices.[9] Extensive investigations have been carried out in inorganic ionic conductors among ionic conductors, such as $LiBH_4$−LiX,[10] $La_{0.62}Li_{0.16}TiO_3$,[11] and $Li_6ALa_2Ta_2O_{12}$.[12] Comparable to inorganic ionic conductors, organic ionic conductors display attractive adjustability of molecular structure, which can be modified by chemical tailored method to fine-tune their physical and chemical properties. Ionic crystals are a class of crystalline compounds containing anions and cations whose properties differ significantly to conventional crystals in electrochemical properties. And their ionic character means that ionic crystals are a class of ionic conductors.[13] Stemming from the large electrochemical window and high charge conductivity of imidazolium-based ionic liquids, Zhu and co-workers modified the molecular structure of ionic liquid to synthesize a small-molecule organic ionic crystal material, 1-methyl-3-acetylimidazolium iodide (MA-II).[14] Using MA-II as matrix for the solid-state electrolyte of DSSC, the highest conversion efficiency of 2.6% was obtained under 0.5 sun irradiation.[14] After that, several organic ionic crystals have been attempted on the solid-state electrolytes of DSSCs, which exhibited excellent electrical properties and promising device performances as good as those of some liquid electrolytes. For instance, an efficiency of 6.3% was reported on *N*-propargyl imidazolium as single-component solid electrolyte.[9] Carbazole−imidazolium iodide was designed for dual hole/triiodide transportation.[15] Ester-functionalized imidazolium provided a three-dimensional channel for iodides.[16] Cyanobiphenyl-functionalized imidazolium, with a tunable conductivity versus alkyl chain length, recorded 6.55% efficiency with light scattering effect under 0.5 sun irradiation.[13] We have also demonstrated a choline iodide organic ionic conductor with 2.5% cell efficiency.[17] However, the study of organic ionic crystals is still in its infancy. Most of the types of such compounds are confined to the imidazolium-based crystals, and then it inevitably limits the research on the conductive mechanism of organic ionic crystals and its application.

Received: August 15, 2014
Accepted: December 3, 2014
Published: December 3, 2014

Consequently, it is crucial to enrich the types of organic ionic crystals for their development. It is very important to explore new organic ionic crystals with excellent physical/chemical properties and derive high photoelectrical performance for the application of organic ionic crystals in DSSCs.

In this work, we design and synthesize a novel type of organic ionic crystal, thiaozole/benzothiaozole-based crystals. A kind of dicationic structure is designed in the crystals (Figure 1). Larger cations are reported to reduce the rate of electron

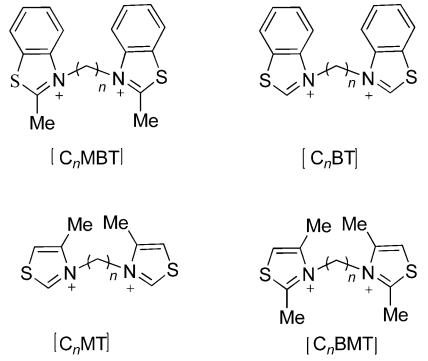

Figure 1. Chemical structures of the cations in thiaozole/benzothiaozole-based dicationic crystals.

recombination and result in an overall improvement in the open-circuit photovoltage.[18,19] To the best of our knowledge, the thiaozole/benzothiaozole-based dicationic conductors in solid-state DSSC have not been studied so far. Compared to the traditional monocationic crystals, the dicationic crystals have a larger size and provide more opportunities to fine-tune their physical/chemical properties. As a consequence, these solid-state electrolyte-based DSSC achieve photoelectric conversion efficiency of 7.90% under full air-mass (AM 1.5) sunlight (100 mW·cm^{-2}).

EXPERIMENTAL SECTION

Materials and Reagents. All chemicals are of analytical reagents (ARs). 4-Methylthiazole, 2,4-dimethylthiazole, benzothiazole, 2-methylbenzothiazole, 1,3-dibromopropane, 1,4-dibromobutane, 1,5-dibromopentane, 1,6-dibromohexane, iodine, 4-*tert*-butylpyridine, 1,2-dimethyl-3-propylimidazolium iodide, and chloroplatinic acid were purchased from Aladdin Industrial Co. and used without any processing. Potassium tetrafluoroborate, acetonitrile, etanol, toluene, ethyl acetate, and diethyl ether were purchased from Sinopharm Chemical Reagent Co., Ltd.. Organic solvents used in this work were purified using the standard process (Part 5 in the Supporting Information). Fluorine-doped tin oxide (FTO) transparent conductive glass was used as the substrate for fabrication of TiO_2 thin film electrode. $TiCl_4$ (AR) was purchased from Tianjin Kemiou Chemical Reagent Co., Ltd.. Dye sensitizer and P25 particles used in this work were purchased from Wuhan Geao Science Instruments Co.

Characterization. NMR and IR spectra were recorded on a Bruker Avance 400 MHz spectrometer and a Bruker Tensor 27 spectrometer, respectively. The XRD measurements were performed on a Rigaku D/Max-RA X-ray diffractometer equipped with graphite-monochromatized high-intensity Cu Kα radiation (λ = 1.5418 Å). The thermal properties of crystals were measured on Thermoanalyzer Systems (Q1000DSC+LNCS+FACS Q600SDT) at a scanning rate of 10 °C·min^{-1} in the temperature range of 20−600 °C under N_2 atmosphere. The melting points were characterized on Micro Melting Point Determination (X5, Beijing Tec. Instrument Co., Ltd.)

The conductivity of the electrolytes was characterized in an ordinary cell composed of Teflon tube and two conductive glass electrodes, which were a square 1 cm on the side, on a CHI660d electrochemical workstation at room temperature, using the alternating current (AC) impedance method over the frequency range of 1 Hz to 1 MHz. The steady-state voltammetry was tested in a photoelectrochemical cell equipped with a 0.05 mm radius platinum ultramicroelectrode as the working electrode, a platinum foil as the counter electrode, and a saturated calomel electrode as reference electrode.

The photocurrent intensity versus photovoltage (J−V) curves of the devices measured under standard AM 1.5 solar illuminations at intensity of 100 mW·cm^{-2} using a Keithley 2400 source meter. The electrochemical impedance spectroscopy (EIS) measurements of devices were tested using the CHI660d electrochemical workstation equipped with three identical stainless steel electrodes as the working, counter, and reference electrodes, respectively, under dark state. The bias voltage for the impedance measurement was −0.70 V and 20 mV AC amplitude signals with frequencies ranging from 0.01 to 10^5 Hz.

Synthesis of Organic Dicationic Crystals. The synthesis procedure was divided into two steps: the coupling reaction of 2-methylbenzothiazole with a dibromoalkane and the anion exchange in water. 3,3′-(Pentane-1,5-diyl)-bis(2-methylbenzothiazolium)-dibromide, [C_5MBT]Br_2, was synthesized as follows: 13.6 mL (0.1 mol) of 1,5-dibromopentane and 2.26 g (0.22 mol) of 2-methylbenzothiazole was added into 250 mL of acetonitrile. The resulting solution was stirred at 120 °C for 72 h under N_2 atmosphere. The resulting mixture was filtered to obtain the solid powder. The crude product was washed by diethyl ether and recrystallized from ethanol. Followed by washing successively with toluene, ethyl acetate, and diethyl ether, the pure products were obtained by vacuum drying at 40 °C for 24 h. ^{1}H NMR (400 MHz, deuterated dimethyl sulfoxide (DMSO-d_6): 8.45 (d, 2H),8.32 (d, 2H), 7.89 (t, 2H), 7.82 (t, 2H), 4.72 (t, 4H), 3.22 (s, 6H), 1.92 (m, 4H), 1.60 (m, 2H). The first step in the synthesis of other compounds in a series of thiaozole/benzothiaozole-based dicationic crystals was similar to that of [C_5MBT]Br_2. The anion exchange step was achieved by a metathesis reaction of the bromide salts with the corresponding anion salts. Bromide salt (0.01 mol) was dissolved in 50 mL of H_2O and treated with 0.02 mol of corresponding anion salt. The resulting solution was stirred at room temperature for 24 h. The solvent was removed by evaporation under reduced pressure. The final product was dried under vacuum at 40 °C for 24 h.

Preparation of Electrolytes. The electrolyte contains organic dicationic crystal matrix, I^- source (1,2-dimethyl-3-propylimidazolium iodide, DMPII), I_2 and charge recombination inhibitor *t*BP (4-*tert*-butylpyridine). The molar proportion of composition was usually 0.1:0.1:0.02:0.01 (crystal matrix/I^- source/I_2/charge recombination inhibitor). All components were mixed in proportion and uniformly ground. The mixture was dried under vacuum at 60 °C and then allowed to cool to room temperature to give a solid-state electrolyte before the characterization and fabrication of DSSC.

Device Fabrication of DSSC. FTO conductive glass was successively washed by ethanol, hydrochloric acid, isopropanol, and anhydrous ethanol in ultrasonic cleaning machine. Two layers of TiO_2 particles were deposited onto cleaned FTO conductive glass and used as working electrode. The glass substrate was treated with 50 mM $TiCl_4$ aqueous solution at 80 °C for 30 min to make a good mechanical contact between the following printed TiO_2 layer and conducting glass matrix. The layer TiO_2 particles were deposited onto the treated FTO conductive glass. The FTO conductive glass was covered at two parallel edges with an adhesive tape to control the thickness of mesoporous TiO_2 film. A 15−25 μm thick film of 20 nm sized P25 particles was deposited onto the FTO conductive glass electrode by the doctor-blade technique. The resulting TiO_2 film was annealed at 450 °C for 30 min. The obtained TiO_2 electrode was cooled to 80 °C and immersed in 0.5 M N719 ethanol solution at room temperature for 24 h to complete the sensitizer loading. The dye-sensitized TiO_2 electrode was washed with anhydrous ethanol and dried in vacuum drying oven at 60 °C for 5 min. To prepare the Pt counter electrode, two drops of 50 mM H_2PtCl_6 in isopropanol were placed onto the cleaned FTO conductive glass substrate, followed by drying and annealing at 380 °C for 30 min.

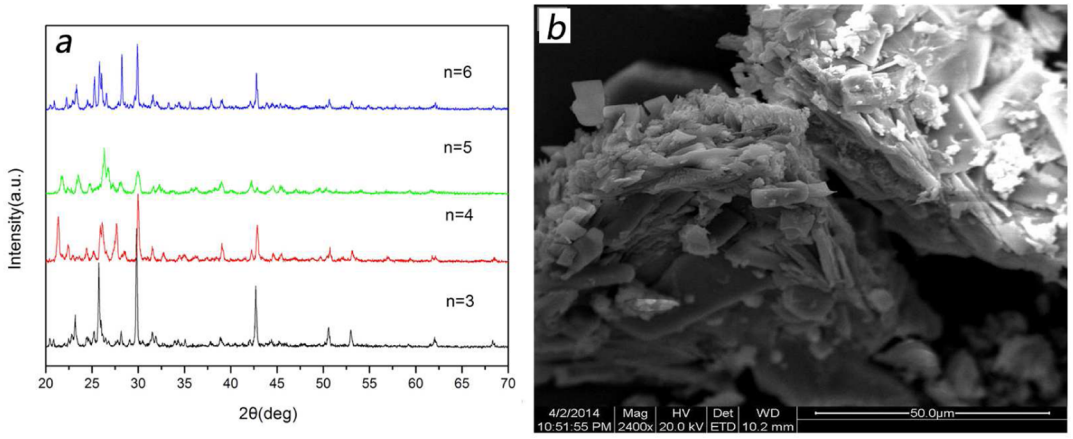

Figure 2. (a) XRD patterns of a series of $[C_nMBT][BF_4]_2$ (n = 3, 4, 5, 6); (b) SEM image of $[C_5MBT][BF_4]_2$.

Solid-state DSSC was fabricated by sandwiching the thiaozolium/benzothiaozolium dicationic crystal-based electrolytes into the space between the dye-sensitized TiO_2 electrode and the Pt counter electrode using the knife-coating method to form a 1 cm^2 area sheet. The two electrodes were clipped together by heat presser (0.18 MPa, 135 °C, 35 s), and a 100 μm thick heat-sealing film was used for the sealing of the cell.

RESULTS AND DISCUSSION

Thermal and Electrochemical Properties of Organic Dicationic Crystals. The crystal properties of the organic dicationic compounds were confirmed by the XRD patterns and SEM images, as shown in Figure 2. All samples with different carbon chain length show strong diffraction peaks. The diffraction angles of major five strongest peaks for different samples are close to each other, suggesting a similar crystal structure. However, because of the lack of standard diffraction data, the crystal structure cannot be determined according to the present patterns. The SEM image shows textured structure and flat surfaces of $[C_5MBT][BF_4]_2$, which is also a clue for the crystal nature of these materials.

Thermal stability is an important factor for evaluating electrolyte materials. Thermal decomposition temperatures were measured by thermogravimetric analysis (TGA). As shown in Figure 3, the series of $[C_nMBT][BF_4]_2$ (n = 3, 4, 5, 6) shows similar decomposition behaviors. They have decomposition temperature at approximately 200 °C. We also measured the melting points of $[C_nMBT][BF_4]_2$ and melting ranges of $[C_nMBT][BF_4]_2$-based electrolytes (Table S1 in Supporting Information).The excellent thermal stability may arise from their high lattic Gibbs energies due to the conformational rigidity of symmetric cations.[5] That is to say, this kind of crystal is thermally stable until ~200 °C, which makes them good candidates for outdoor applications of solar cells.

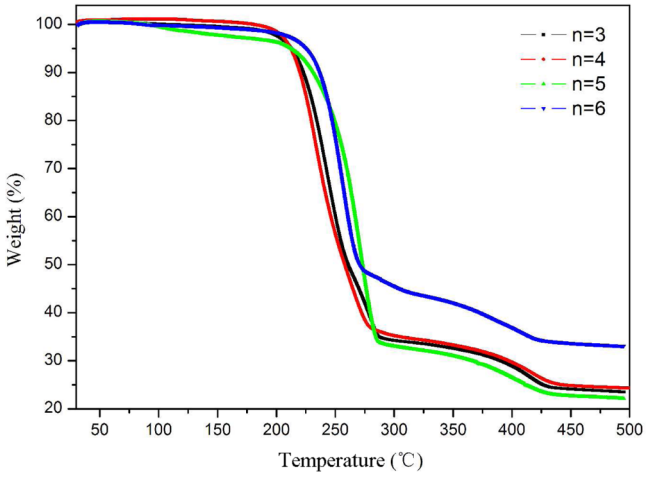

Figure 3. TGA curves of a series of $[C_nMBT][BF_4]_2$ (n = 3, 4, 5, 6).

It is well-known that the efficiency and the fill factor of DSSC are critically dependent on the ion conductivity of the electrolyte applied in the cell.[20,21] In our experiments, the ion conductivities of $[C_nMBT][BF_4]_2$ (n = 3, 4, 5, 6)-based electrolytes were characterized by the EIS technique (Figure 4).

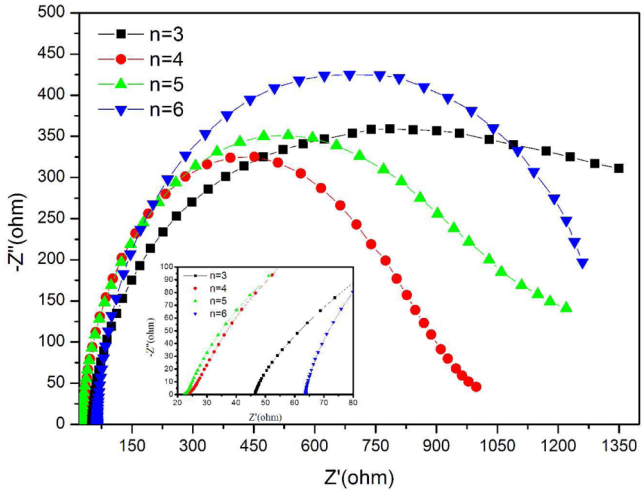

Figure 4. Nyquist plots for $[C_nMBT][BF_4]_2$ (n = 3, 4, 5, 6).

The EIS Nyquist plot of the electrolyte is oblique lines at high frequency range, and the intercept of the inclined line with real axis is considered as the bulk resistance.[22] The conductivity was calculated using the following equation:

$$\sigma = l/RS \quad (1)$$

where σ is the conductivity in S/cm, R is the ohmic resistance of the electrolyte, l is the distance between the two electrodes, and S is the area of the electrodes. The ion conductivities were calculated, and the results were summarized in Table 1. As can be seen from Figure 4, the bulk resistances of the $[C_nMBT]$-

dx.doi.org/10.1021/am5053762 | ACS Appl. Mater. Interfaces 2014, 6, 22088−22095

Table 1. Ionic Conductivity and D_{app} of I^-/I_3^- of the Solid-State Electrolytes

electrolyte	conductivity [10^{-4} S/cm]	I_{ss} (I^-) [10^{-7} A]	D_{app} (I^-) [10^{-8}cm^2/S]	I_{ss} (I_3^-) [10^{-7}A]	D_{app} (I_3^-) [10^{-7} cm^2/S]
$[C_3MBT][BF_4]_2$	2.15	0.455	0.275	2.690	1.4636
$[C_4MBT][BF_4]_2$	4.25	2.680	1.620	6.260	3.4054
$[C_5MBT][BF_4]_2$	4.44	1.890	1.143	8.900	4.8416
$[C_6MBT][BF_4]_2$	1.56	0.420	0.254	0.807	0.4390
$[C_5BT][BF_4]_2$	3.73	0.391	0.236	1.680	0.9139
$[C_5MT][BF_4]_2$	1.28	0.113	0.068	0.793	0.4314
$[C_5BMT][BF_4]_2$	1.37	0.266	0.161	0.893	0.4858

$[BF_4]_2$ (n = 3, 4, 5, 6)-based electrolytes significantly decrease first with the value of n increasing from 3 to 5, but then sharply increase as the value of n is equal to 6. The changing trend of the ion conductivities is opposite to that of the bulk resistances according to eq 1. Concretely, the ion conductivities increase from 2.15 × 10^{-4} to 4.44 × 10^{-4} S·cm^{-1} when the value of n increases from 3 to 5 and then decreases to 1.56 × 10^{-4} S/cm as n is equal to 6. The $[C_5MBT][BF_4]_2$-based electrolyte exhibited the highest ion conductivity among the $[C_nMBT][BF_4]_2$ (n = 3, 4, 5, 6)-based solid-state electrolytes. It has been demonstrated that the $\pi-\pi$ stacked aromatic rings can provide the charge transport from the counter electrode to the photoelectrode.[2,21,23,24] We suppose that $[C_5MBT][BF_4]_2$ can form a favorable ion-conductive channel in the electrolyte due to the relatively suitable saturated carbon chain.[13,25] It is the appropriate ion-conductive channel that leads to the high ion conductivity of the $[C_5MBT][BF_4]_2$-based electrolyte. However, the $[C_6MBT][BF_4]_2$-based electrolyte shows a lower ion conductivity. It may be explained by the reduction of the ion-conductivity layer number per unit length if the mobility of the ionic species in the layer is the same in the salts.[25]

The diffusion of triiodide is also one of the limiting factors for the high performance of DSSC.[3] Lin's group reported that the ionic diffusion can reflect the demand for high-performance solid-state DSSC more correctly than ion conductivity.[26] Steady-state voltammograms of the $[C_nMBT][BF_4]_2$ (n = 3, 4, 5, 6)-based electrolytes were investigated (Figure 5). The apparent diffusion coefficients (D_{app}) of I^- and I_3^- were calculated from the anodic and cathodic steady-state current I_{ss} by using the following equation:

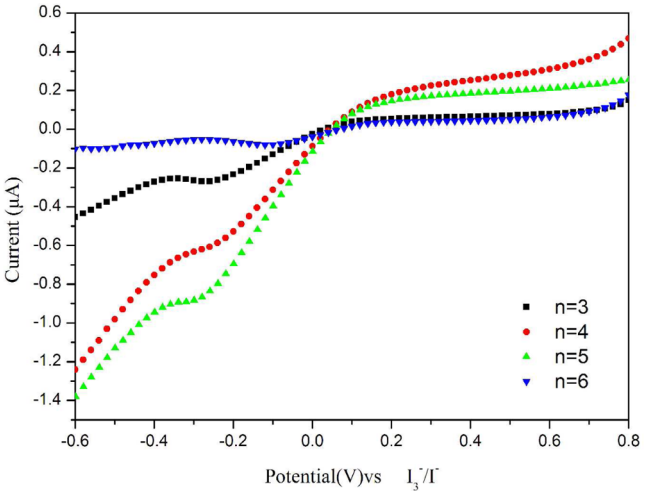

Figure 5. Steady-state voltammograms of the $[C_nMBT][BF_4]_2$ (n = 3, 4, 5, 6)-based electrolytes at a scan rate of 10 mV·s^{-1}.

$$I_{ss} = 4nrFCD_{app} \quad (2)$$

where n is the number of electrons per molecule, F is the Faraday constant, C is the concentration, and r is the radius of the electrode. The calculated diffusion coefficients of I^- and I_3^- were summarized in Table 3. The changing trend in D_{app} of the I^-/I_3^- redox couple is similar to that of the ion conductivity, and the $[C_5MBT][BF_4]_2$-based electrolyte shows the highest D_{app} (I_3^-) of 4.8416 × 10^{-7} cm^2/S.

It has been reported that the shape of the anion has a significant influence on the cation geometry, thus directing the crystalline packing of the resulting salt.[27] To gain an insight into the effect of the anion on the electrochemical property of organic dicationic crystal, we investigated the ion conductivity and apparent diffusion coefficient of $[C_5MBT]Br_2$-based electrolyte (Table S2 in Supporting Information). Its conductivity and D_{app} (I_3^-) are 2.00 × 10^{-4} S/cm and 4.8416 × 10^{-7} cm^2/S, respectively. The results were not better than those of $[C_5MBT][BF_4]_2$.

Early work has indicated that the cations in the electrolyte have a great influence on the photovoltaic parameters of DSSC.[3] For example, lithium ions doped in the electrolyte can interact with TiO_2 surface and reduce the conduction band energy level, which in turn leads to the increase of short-circuit current and the decrease of open-circuit voltage.[28,29] To understand the influence of the cation structure of the dicationic organic crystals on the electrochemical property of crystal, the other three dicationic crystals with the different substituted thiazole units were prepared for comparison, such as $[C_5BT][BF_4]_2$, $[C_5MT][BF_4]_2$, and $[C_5BMT][BF_4]_2$ (Table 1). Among them, $[C_5BT][BF_4]_2$ most similar to $[C_5MBT][BF_4]_2$ in structure shows the highest ion conductivity (3.73 × 10^{-4} S/cm) and D_{app} (I_3^-) (0.9139 × 10^{-7} cm^2/S), which are still lower than those of $[C_5MBT][BF_4]_2$. The lower triiodide diffusion efficiencies are obtained for the $[C_5MT][BF_4]_2$- and $[C_5BMT][BF_4]_2$-based electrolytes. The electrostatic forces between the cation and anion are stronger in the crystals of $[C_5MT][BF_4]_2$ and $[C_5BMT][BF_4]_2$ compared to those in $[C_5MBT][BF_4]_2$ and $[C_5BT][BF_4]_2$. The stronger electrostatic force is one of the reasons for the decreased triiodide diffusion efficiency.[3]

Interfacial Compatibility of Electrolyte. It has been concluded that the interfacial compatibility of electrolyte is another main factor affecting the photovoltaic efficiency of DSSC.[30] There must be good penetration of the electrolyte into the TiO_2 pores, which leads to the good contact between the solid-state electrolyte and the dye-sensitized TiO_2 electrode.[31] So, SEM technique is used for the characterization. Typical SEM images for the cross sections of photoanode casted with $[C_5MBT][BF_4]_2$-based electrolyte before and after heat press are shown in Figure 6. Two layers of TiO_2 photoanode and electrolyte along with a distinct interface

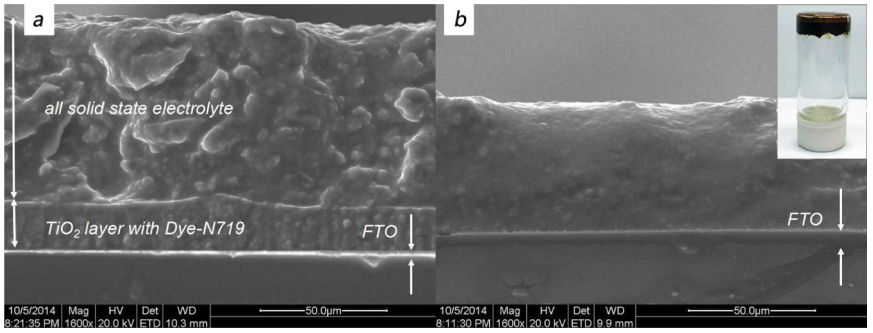

Figure 6. Cross section SEM image of photoanode with solid-state electrolyte before (a) and after (b) heat press. The composition of $[C_5MBT][BF_4]_2$-based electrolyte is 0.1 mol $[C_5MBT][BF_4]_2$ + 0.1 mol DMPII + 0.02 mol I_2 + 0.01 mol TBP. (inset) Digital camera image of the solid-state electrolyte.

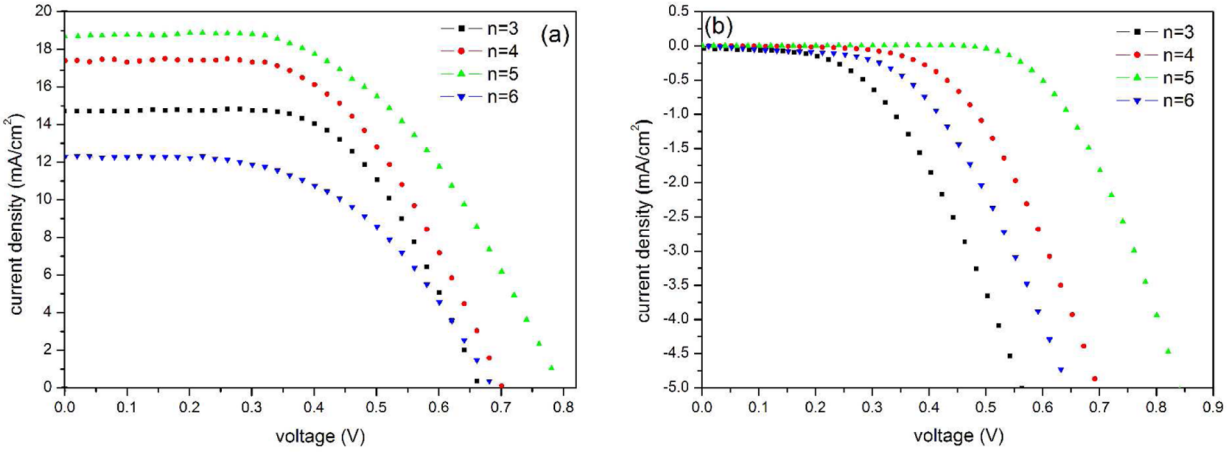

Figure 7. J–V curves of devices based on the electrolytes using $[C_nMBT][BF_4]_2$ (n = 3, 4, 5, 6) as matrixes (a) under 1.5 sun light intensity illumination (b) in dark conditions.

between the layers can be well-observed before heat press (Figure 6a), while after heat press, the total thickness of photoanode plus electrolyte shrinks apparently. The interface between photoanode and electrolyte also disappears. Furthermore, the cross section of photoanode tends to be more smooth (Figure 6b). We attribute the phenomenon to the fillings of electrolyte into the mesopores in the TiO_2 photoanodes. After combined with DMPII, iodine, the electrolyte mixtures have a melting temperature ranging from 110 to 135.7 °C as detected on a micro melting point detector (Table S1). The electrolyte is transformed to liquid and pressed at 135 °C under 0.18 MPa for 35 s. Fluidic liquid is suggested to penetrate through the TiO_2 pore and form good contact without difficulty.[32] So a good contact between the dye-sensitized TiO_2 and solid-state electrolyte is achieved.

Characterization of DSSCs. All solid-state DSSCs were fabricated. Figure 7 shows the J–V curves of devices based on the electrolytes using $[C_nMBT][BF_4]_2$ (n = 3, 4, 5, 6) as matrixes under 1 sun light intensity illumination and under dark conditions. Their photovoltaic performances were summarized in Table 2. For the DSSC using $[C_5MBT][BF_4]_2$ as matrix for the electrolyte, the conversion efficiency, open-circuit voltage (V_{oc}), short-current density (J_{sc}) under AM 1.5 100 mW·cm^{-2} are 7.90%, 0.794 V, and 18.78 mA·cm^{-2}, respectively. The conversion efficiency and open-circuit voltage of the $[C_4MBT][BF_4]_2$-based electrolyte are slightly weaker than those of $[C_5MBT][BF_4]_2$-based electrolyte.

Table 2. Device Performances of DSSCs with Different Electrolytes

electrolytes	J_{sc} [mA·cm^{-2}]	V_{oc} [V]	*FF* [%]	*PCE* [%]
$[C_3MBT][BF_4]_2$/DMPII/I_2	14.90	0.665	59.88	5.93
$[C_4MBT][BF_4]_2$/DMPII/I_2	17.40	0.699	55.12	6.70
$[C_5MBT][BF_4]_2$/DMPII/I_2	18.78	0.794	52.90	7.90
$[C_6MBT][BF_4]_2$/DMPII/I_2	12.26	0.685	52.66	4.42
$[C_5BT][BF_4]_2$/DMPII/I_2	9.02	0.627	70.55	3.99
$[C_5MT][BF_4]_2$/DMPII/I_2	4.25	0.704	58.83	1.76
$[C_5BMT][BF_4]_2$/DMPII/I_2	5.36	0.742	58.84	2.34

The value of V_{oc} for DSSC with I^-/I_3^- redox electrolyte can be represented by the following equation:[33]

$$V_{oc} = \frac{kT}{e}\ln\left(\frac{I_{inj}}{n_{cb}k_{et}[I_3^-]}\right) \quad (3)$$

where k and T are the Boltzmann constant and absolute temperature, respectively, I_{inj} is the injection current from dye to semiconductor, n_{cb} is the electron density on the conduction band of the semiconductor, and k_{et} is the rate constant for I_3^- reduction. According to eq 3, the highest V_{oc} of the $[C_5MBT][BF_4]_2$-based electrolyte is related to the suppression of the dark current at the TiO_2 electrode/electrolyte interface.[34] The dark current originates from the reduction of triiodide by conduction band electrons from TiO_2.[35] At the interface of the dye-sensitized TiO_2 photoanode and electrolyte, a higher

dx.doi.org/10.1021/am5053762 | ACS Appl. Mater. Interfaces 2014, 6, 22088–22095

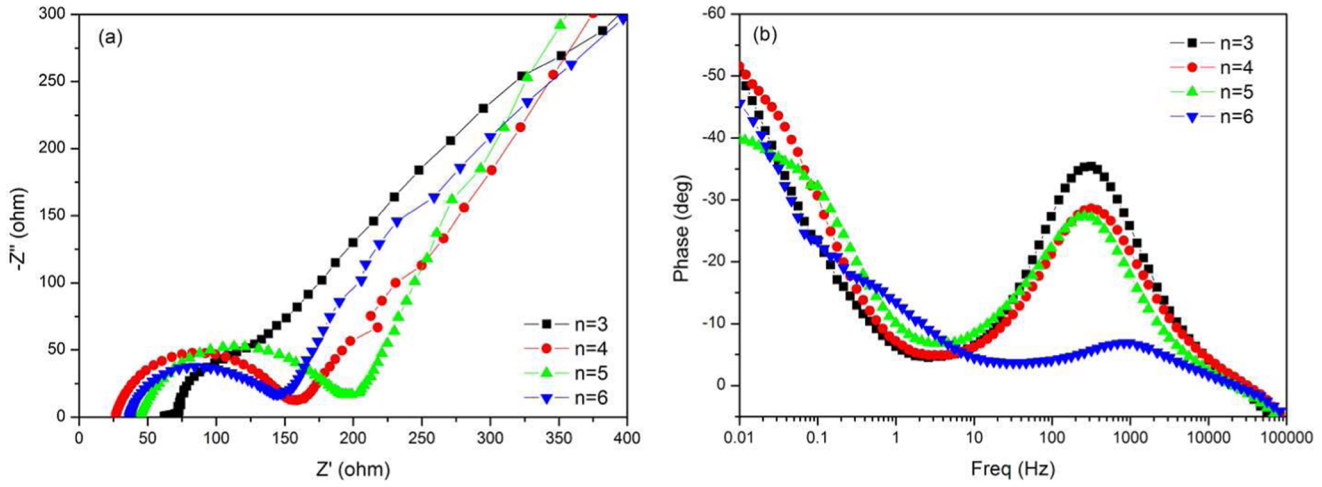

Figure 8. (a) Nyquist plots and (b) fitted Bode phase plots of the devices with $[C_nMBT][BF_4]_2$ (n = 3, 4, 5, 6)-based electrolytes under dark condition.

diffusion coefficient of triiodide can promote the transport of triiodide to the Pt counterelectrode for the iodide form, thus ensuring a lower triiodide reduction rate (k_{et}) and a higher V_{oc}.[36] As shown in Figure 7b, the onset of dark current has a positive shift of ~150 mV from the $[C_4MBT][BF_4]_2$-based electrolyte to $[C_5MBT][BF_4]_2$-based electrolyte. The rise of dark current is attributed to the higher conductivity and triiodide diffusion coefficient in the $[C_5MBT][BF_4]_2$-based electrolyte.

Furthermore, it can be seen from Table 2 that the performances of the devices using the other three crystals with the different substituted thiazole units as matrixes for electrolytes are obviously worse than those of the device with $[C_5MBT][BF_4]_2$. (The J–V curves of the above devices are given in the Supporting Information, Figure S11.) The V_{oc} of device with $[C_5BT][BF_4]_2$ (0.627 V) is much lower than the value of device with $[C_5MBT][BF_4]_2$ (0.794 V). It also has been previously observed by other researchers that bulkiness of the head part of cation present in electrolyte can affect the open-circuit voltage.[37]

To further verify the positive effect of the dicationic structure of crystals on device performance, we prepared monocationic 1-methyl-3-amylbenzothiazolium bromide. For the DSSC using it as matrix for the electrolyte, the conversion efficiency, open-circuit voltage (V_{oc}), short-current density (J_{sc}) under AM 1.5 100 mW·cm^{-2} are 2.47%, 0.591 V, and 9.51 mA·cm^{-2}, respectively (Figure S13 and Table S3 in Supporting Information). The results show that the dicationic structure of crystals with large size is indeed beneficial for the better device performance.

Note that the variance in J_{sc} values cannot be attributed solely to the change of ion conductivities or D_{app} of I^-/I_3^- of electrolytes applied in this work. We can easily find that it is not the simple correspondence between the variety in J_{sc} values and the change of ion conductivity or change of D_{app} of I^-/I_3^- from Tables 1 and 2. Wang and co-workers reported the alkyl length of the solid electrolyte can not only influence the electron injection yield but also influence charge collection efficiency, which all lead to the change of short-current density.[2]

Electrochemical impedance spectroscopy (EIS) measurements have been undertaken to investigate electronic and ionic processes in DSSC.[38] In general, three typical characterization frequency peaks in the Bode phase plot or three typical semicircles in the Nyquist plot can be observed.[39,40] In the Nyquist plots, the semicircle occurring at highest frequencies (100–10^4 Hz) corresponds to the redox reactions of the platinum counterelectrode; the semicircle at medium frequencies (1–100 Hz) is related to photoinjected electron transfer in the TiO_2 or back reaction from the injected electron in the TiO_2 to the electrolyte; the lowest-frequency semicircle is attributed to the Nernst diffusion of the redox within the electrolyte (0.01–1 Hz).[41] Figure 8 shows the impedance spectra of DSSCs using $[C_nMBT][BF_4]_2$ (n = 3, 4, 5, 6) as matrixes for electrolytes under dark condition. The figures were given in the forms of Nyquist and Bode plots. The corresponding resistance values of $[C_nMBT][BF_4]_2$ (n = 3, 4, 5, 6)-based electrolytes are listed in Table 3. The equivalent circuit of this model (Figure S15 Supporting Information) has been already reported.[41−44] The dark reaction impedance of the medium frequency semicircle in the Nyquist plot reveals the electron recombination at the dye-sensitized TiO_2 electrode/electrolyte interface, which is caused by the conduction band electrons of the mesoscopic TiO_2 electrode captured by I_3^- ions.[20] It can be clearly seen that the R_2 (the resistance of the dye-sensitized TiO_2 electrode/electrolyte) values show the same changing trend with that of ion conductivity for $[C_nMBT][BF_4]_2$ (n = 3, 4, 5, 6)-based electrolytes. It increases with the increase of the value of n and reaches a maximum of 154.8 Ω as n equals 5. It indicates that the recombination process between the conduction band electrons in the dye-sensitized TiO_2 electrode and electrolyte is more inhibited. This result is consistent with that of the dark current characterization. There are linear behaviors in the low-frequency range, demonstrating that there is slow ionic diffusion in the $[C_nMBT][BF_4]_2$ (n = 3, 4, 5, 6)-based electrolytes. It can be concluded that carrier transport in the solid-state electrolyte is mainly from ionic diffusion conduction.[39]

The effective lifetime of the electron (τ_e) before recombination in the dye-sensitized TiO_2 electrode can be related to the inverse of the characteristic frequency and is estimated by the following equation:[45]

$$\tau_e = \frac{1}{\omega_{max}} = \frac{1}{2\pi f_{max}} \quad (4)$$

where f_{max} is the maximum frequency of the midfrequency peak of the Bode phase plot. The f_{max} and lifetime of the electron were also summarized in Table 3. The electron lifetimes for

Table 3. Parameters Obtained by the EIS of the Devices Fabricated with Different Electrolytes

electrolyte	R_s [Ω]	R_2 [Ω]	f_{max} [Hz]	τ_e [ms]
$[C_3MBT][BF_4]_2$/DMPII/I_2	62.10	85.9	0.0316	5.039
$[C_4MBT][BF_4]_2$/DMPII/I_2	26.88	130.7	0.0147	10.832
$[C_5MBT][BF_4]_2$/DMPII/I_2	43.67	152.6	0.0121	13.159
$[C_6MBT][BF_4]_2$/DMPII/I_2	36.27	111.1	0.0825	1.930

recombination (τ_e) of the $[C_4MBT][BF_4]_2$- and $[C_5MBT][BF_4]_2$-based electrolytes are 10.832 and 13.159 ms, respectively. Therefore, it can be concluded that $[C_5MBT][BF_4]_2$-based electrolyte yields a longer electron recombination lifetime, which favors electron transport over a longer distance with less diffusive hindrance and finally leads to enhanced photoconversion efficiency.[46]

The incident photon-to-current conversion efficiency (IPCE) curves of these DSSCs with $[C_nMBT][BF_4]_2$ (n = 3, 4, 5, 6)-based electrolytes are shown in Figure 9. The maximum IPCE

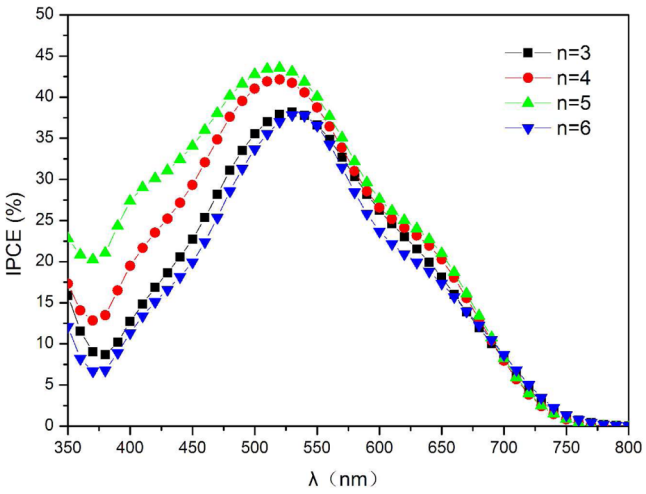

Figure 9. IPCE curves of the devices with $[C_nMBT][BF_4]_2$ (n = 3, 4, 5, 6)-based electrolytes.

value at 530 nm is 38.17%, 42.13%, 43.55%, and 37.86% for $[C_3MBT][BF_4]_2$, $[C_4MBT][BF_4]_2$, $[C_5MBT][BF_4]_2$- and $[C_6MBT][BF_4]_2$-based electrolytes, respectively. The integration of IPCE is in good agreement with J_{sc}, both of which indicate the superior properties of $[C_5MBT][BF_4]_2$ in the present work.

CONCLUSIONS

In conclusion, a novel kind of benzothiaozole-based organic dicationic crystal with large cations and good adjustability of molecular structure are designed and applied in DSSCs. We studied the influence of crystal structure on the electrochemical properties and device performances. The results show that $[C_5MBT][BF_4]_2$ is the effective matrix of electrolyte for solid-state DSSCs. A cell efficiency of 7.90% is recorded on the optimized condition. The high efficiency benefits from the highest ion conductivity and long electron lifetime. The present research work develops a promising kind of organic ionic crystal and an effective solid-state electrolyte for DSSCs.

ASSOCIATED CONTENT

Supporting Information

NMR and IR curves of electrolytes and contrast experimental results. This material is available free of charge via the Internet at http://pubs.acs.org.

AUTHOR INFORMATION

Corresponding Author

*E-mail: wangyefeng@snnu.edu.cn.

Notes

The authors declare no competing financial interest.

ACKNOWLEDGMENTS

This work was supported by the Natural Science Foundation of China (No. 21071093) and Fundamental Research Funds for the Central Universities (Grant No. GK201402017, GK201101004) from the Department of Education.

REFERENCES

(1) Yella, A.; Lee, H. W.; Tsao, H. N.; Yi, C.; Chandiran, A. K.; Nazeeruddin, M. K.; Diau, E. W.; Yeh, C. Y.; Zakeeruddin, S. M.; Grätzel, M. Porphyrin-Sensitized Solar Cells with Cobalt (II/III)-Based Redox Electrolyte Exceed 12% Efficiency. *Science* **2011**, *334*, 629−634.

(2) Grätzel, M. Photoelectrochemical Cells. *Nature* **2001**, *414*, 338−344.

(3) Wyss, P.; Moehl, T.; Zakeeruddin, S. M.; Grätzel, M. Influence of Cations of the Electrolyte on the Performance and Stability of Dye Sensitized Solar Cells. *J. Mater. Chem.* **2012**, *22*, 24424−24429.

(4) Mathew, S.; Yella, A.; Gao, P.; Humphry-Baker, R.; Curchod, B. F. E.; Ashari-Astani, N.; Tavernell, I.; Rothlisberger, U.; Nazeeruddin, Md. K.; Grätzel, M. Dye-Sensitized Solar Cells with 13% Efficiency Achieved Through the Molecular Engineering of Porphyrin Sensitizers. *Nat. Chem.* **2014**, *6*, 242−247.

(5) Bu, Y.; Cao, Y.; Zhang, J.; Wang, M.; Li, R.; Wang, P.; Zakeeruddin, S. M.; Grätzel, M. High-Performance Dye-Sensitized Solar Cells Based on Solvent-Free Electrolytes Produced from Eutectic Melts. *Nat. Mater.* **2008**, *7*, 626−630.

(6) Li, D.; Qin, D.; Deng, M.; Luo, Y.; Meng, Q. Optimization the Solid-State Electrolytes for Dye-Sensitized Solar Cells. *Energy Environ. Sci.* **2009**, *2*, 283−291.

(7) Wu, J. H.; Hao, S. C.; Lan, Z.; Lin, J. M.; Huang, Y. F.; Li, P. J.; Yin, S.; Sato, T. An All-Solid-State Dye-Sensitized Solar Cell-Based Poly(N-alkyl-4-vinyl-pyridine iodide) Electrolyte with Efficiency of 5.64%. *J. Am. Chem. Soc.* **2008**, *130*, 11568−11569.

(8) Knauth, P. Inorganic Solid Li Ion Conductors: An Overview. *Solid State Ionics* **2009**, *180*, 911−916.

(9) Wang, H.; Li, J.; Gong, F.; Zhou, G.; Wang, Z. S. Ionic Conductor with High Conductivity as Single-Component Electrolyte for Efficient Solid-State Dye-Sensitized Solar Cells. *J. Am. Chem. Soc.* **2013**, *135*, 12627−12633.

(10) Maekawa, H.; Matsuo, M.; Takamura, H.; Ando, M.; Noda, Y.; Karahashi, T.; Orimo, S. Halide-Stabilized $LiBH_4$, a Room-Temperature Lithium Fast-Ion Conductor. *J. Am. Chem. Soc.* **2009**, *131*, 894−895.

(11) Yashima, M.; Itoh, M.; Inaguma, Y.; Morii, Y. Crystal Structure and Diffusion Path in the Fast Lithium-Ion Conductor $La_{0.62}Li_{0.16}TiO_3$. *J. Am. Chem. Soc.* **2005**, *127*, 3491−3495.

(12) Thangadurai, V.; Weppner, W. $Li_6ALa_2Ta_2O_{12}$ (A = Sr, Ba): Novel Garnet-Like Oxides for Fast Lithium Ion Conduction. *Adv. Funct. Mater.* **2005**, *15*, 107−112.

(13) Cao-Cen, H.; Zhao, J.; Qiu, L.; Xu, D.; Li, Q.; Chen, X.; Yan, F. High Performance All-Solid-State Dye-Sensitized Solar Cells Based on Cyanobiphenyl-Functionalized Imidazolium-Type Ionic Crystals. *J. Mater. Chem.* **2012**, *22*, 12842−12850.

(14) Zhao, Y.; Zhai, J.; He, J.; Chen, X.; Chen, L.; Zhang, L.; Tian, Y.; Jiang, L.; Zhu, D. High-Performance All-Solid-State Dye-Sensitized Solar Cells Utilizing Imidazolium-Type Ionic Crystal as Charge Transfer Layer. *Chem. Mater.* **2008**, *20*, 6022−6028.
(15) Midya, A.; Xie, Z.; Yang, J.; Chen, Z.; Blackwood, D.; Wang, J.; Adams, S.; Loh, K. P. A New Class of Solid State Ionic Conductors for Application in All Solid State Dye Sensitized Solar Cells. *Chem. Commun.* **2010**, *46*, 2091−2093.
(16) Wang, H.; Zhang, X.; Gong, F.; Zhou, G.; Wang, Z. S. Novel Ester-Functionalized Solid-State Electrolyte for Highly Efficient All-Solid-State Dye-Sensitized Solar Cells. *Adv. Mater.* **2012**, *24*, 121−124.
(17) Wang, Y. F.; Zhang, J. M.; Cui, X. R.; Yang, P. C.; Zeng, J. H. A Novel Organic Ionic Plastic Crystal Electrolyte for Solid-State Dye-Sensitized Solar Cells. *Electrochim. Acta* **2013**, *112*, 247−251.
(18) Kopidakis, N.; Neale, N. R.; Frank, A. J. Effect of an Adsorbent on Recombination and Band-Edge Movement in Dye-Sensitized TiO_2 Solar Cells: Evidence for Surface Passivation. *J. Phys. Chem. B* **2006**, *110*, 12485−12489.
(19) Kusama, H.; Orita, H.; Sugihara, H. TiO_2 Band Shift by Nitrogen-Containing Heterocycles in Dye-Sensitized Solar Cells: a Periodic Density Functional Theory Study. *Langmuir* **2008**, *24*, 4411−4419.
(20) Zhang, X.; Yang, H.; Xiong, H. M.; Li, F. Y.; Xia, Y. Y. A Quasi-Solid-State Dye-Sensitized Solar Cell Based on the Stable Polymer-Grafted Nanoparticle Composite Electrolyte. *J. Power Sources* **2006**, *160*, 1451−1455.
(21) Chen, X.; Zhao, J.; Zhang, J.; Qiu, L.; Xu, D.; Zhang, H.; Han, X.; Sun, B.; Fu, G.; Zhang, Y.; Yan, F. Bis-Imidazolium Based Poly(ionic liquid) Electrolytes for Quasi-Solid-State Dye-Sensitized Solar Cells. *J. Mater. Chem.* **2012**, *22*, 18018−18024.
(22) Shi, Y.; Zhan, C.; Wang, L.; Ma, B.; Gao, R.; Zhu, Y.; Qiu, Y. The Electrically Conductive Function of High-Molecular Weight Poly(ethylene oxide) in Polymer Gel Electrolytes Used for Dye-Sensitized Solar Cells. *Phys. Chem. Chem. Phys.* **2009**, *11*, 4230−4235.
(23) Wang, G.; Wang, L.; Zhou, S.; Fang, S.; Lin, Y. An Iodine-Free Electrolyte Based on Ionic Liquid Polymers for All-Solid-State Dye-Sensitized Solar Cells. *Chem. Commun.* **2011**, *47*, 2700−2702.
(24) Coropceanu, V.; Nakano, T.; Gruhn, N. E.; Kwon, O.; Yade, T.; Katsukawa, K. Brédas, Probing Charge Transport in π-Stacked Fluorene-Based Systems. *J. Phys. Chem. B* **2006**, *110*, 9482−9487.
(25) Xu, F.; Matsumoto, K.; Hagiwara, R. Effects of Alkyl Chain Length on Properties of 1-Alkyl-3-methylimidazolium Fluorohydrogenate Ionic Liquid Crystals. *Chem.—Eur. J.* **2010**, *16*, 12970−12976.
(26) Zhou, Y.; Xiang, W.; Chen, S.; Fang, S.; Zhou, X.; Zhang, J.; Lin, Y. Improvements of Photocurrent by Using Modified SiO_2 in the Poly(ether urethane)/Poly(ethylene oxide) Polymer Electrolyte for All-Solid-State Dye-Sensitized Solar Cells. *Chem. Commun.* **2009**, 3895−3897.
(27) Wang, X.; Vogel, C. S.; Heinemann, F. W.; Wasserscheid, P.; Meyer, K. Solid-State Structures of Double-Long-Chain Imidazolium Ionic Liquids: Influence of Anion Shape on Cation Geometry and Crystal Packing. *Cryst. Growth Des.* **2011**, *11*, 1974−1988.
(28) Kambe, S.; Nakade, S.; Kitamura, T.; Wada, Y.; Yanagida, S. Influence of the Electrolytes on Electron Transport in Mesoporous TiO_2-Electrolyte Systems. *J. Phys. Chem. B* **2002**, *106*, 2967−2972.
(29) Haque, S.; Tachibana, Y.; Willis, R. L.; Moser, J. E.; Grätzel, M.; Klug, D. R.; Durrant, J. R. Parameters Influencing Charge Recombination Kinetics in Dye-Sensitized Nanocrystalline Titanium Dioxide Films. *J. Phys. Chem. B* **2000**, *104*, 538−547.
(30) Zakeeruddin, S. M.; Grätzel, M. Solvent-Free Ionic Liquid Electrolytes for Mesoscopic Dye-Sensitized Solar Cells. *Adv. Funct. Mater.* **2009**, *19*, 2187−2202.
(31) Pringle, J. M. Recent Progress in the Development and Use of Organic Ionic Plastic Crystal Electrolyte. *Phys. Chem. Chem. Phys.* **2013**, *15*, 1339−1351.
(32) De Freitas, J. N.; Nogueira, A. F.; De Paoli, M. A. New Insights into dye-sensitized solar cells with polymer electrolytes. *J. Mater. Chem.* **2009**, *19*, 5279−5294.
(33) Hagfeldt, A.; Grätzel, M. Light-Induced Redox Reactions in Nanocrystalline Systems. *Chem. Rev.* **1995**, *95*, 49−68.
(34) Wang, P.; Zakeeruddin, S. M.; Comte, P.; Charvet, R.; Humphry-Baker, R.; Grätzel, M. Enhance the Performance of Dye-Sensitized Solar Cells by Co-grafting Amphiphilic Sensitizer and Hexadecylmalonic Acid on TiO_2 Nanocrystals. *J. Phys. Chem. B* **2003**, *107*, 14336−14341.
(35) Nazeeruddin, M. K.; Kay, A.; Rodicio, I.; Humphry-Baker, R.; Mueller, E.; Liska, P.; Vlachopoulos, N.; Grätzel, M. Conversion of Light to Electricity by cis-X_2Bis(2,2′-bipyridyl-4,4′-dicarboxylate)-ruthenium(11) Charge-Transfer Sensitizers (X = Cl^-, Br^-, I^-, CN^-, and SCN^-) on Nanocrystalline TiO_2 Electrodes. *J. Am. Chem. Soc.* **1993**, *115*, 6382−6390.
(36) Zhao, J.; Shen, X.; Yan, F.; Qiu, L.; Lee, S.; Sun, B. Solvent-Free Ionic Liquid/Poly(ionic liquid) Electrolytes for Quasi-Solid-State Dye-Sensitized Solar Cells. *J. Mater. Chem.* **2011**, *21*, 7326−7330.
(37) Jeon, S.; Jo, Y.; Kim, K. J.; Jun, Y.; Han, C. H. High Performance Dye-Sensitized Solar Cells with Alkylpyridinium Iodide Salts in Electrolytes. *ACS Appl. Mater. Interfaces* **2011**, *3*, 512−516.
(38) Wang, Q.; Moser, J. E.; Grätzel, M. Electrochemical Impedance Spectroscopic Analysis of Dye-Sensitized Solar Cells. *J. Phys. Chem. B* **2005**, *109*, 14945−14953.
(39) Kern, R.; Saatrawan, R.; Ferber, J.; Stangl, R.; Luther, J. Modeling and Interpretation of Electrical Impedance Spectra of Dye Solar Cells Operated Under Open-Circuit Conditions. *Electrochim. Acta* **2002**, *47*, 4213−4225.
(40) Kuang, D. B.; Klein, C.; Zhang, Z. P.; Ito, S.; Moser, J. E.; Zakkeeruddin, S. M.; Grätzel, M. Stable, High-Efficiency Ionic-Liquid-Based Mesoscopic Dye-Sensitized Solar Cells. *Small* **2007**, *3*, 2094.
(41) Zhao, Y.; Zhai, J.; Wei, T.; Jiang, L.; Zhu, D. Enhanced Photoelectrical Performance of TiO_2 Electrodes Integrated with Microtube-Network Structures. *J. Mater. Chem.* **2007**, *17*, 5084−5089.
(42) Longo, C.; Nogueira, A. F.; De PPaoli, M. A.; Cachet, H. Solid-State and Flexible Dye-Sensitized TiO_2 Solar Cells: a Study by Electrochemical Impedance Spectroscopy. *J. Phys. Chem. B* **2002**, *106*, 5925−5930.
(43) Park, N. G.; Kim, K. M.; Kang, M. G.; Ryu, K. S.; Chang, S. H.; Shin, Y. J. Chemical Sintering of Nanoparticles: A Methodology for Low-Temperature Fabrication of Dye-Sensitized TiO_2 Films. *Adv. Mater.* **2005**, *17*, 2349−2353.
(44) Huang, X.; Qin, D.; Zhang, X.; Luo, Y.; Huang, S.; Li, D.; Meng, Q. The Potential of Eutectic Mixtures as Environmentally Friendly, Solvent-Free Electrolytes for Dye-Sensitized Solar Cells. *RSC Adv.* **2013**, *3*, 6922−6929.
(45) Hou, Q.; Zheng, Y.; Chen, J. F.; Zhou, W.; Deng, J.; Tao, X. Visible-Light-Response Iodine-Doped Titanium Dioxide Nanocrystals for Dye-Sensitized Solar Cells. *J. Mater. Chem.* **2011**, *21*, 3877−3883.
(46) Xia, J.; Masaki, N.; Cantu-Lira, M.; Kim, Y.; Jiang, K.; Yanagida, S. Influence of Doped Anions on Poly(3,4-ethylenedioxythiophene) as Hole Conductors for Iodine-Free Solid-State Dye-Sensitized Solar Cells. *J. Am. Chem. Soc.* **2008**, *130*, 1258−1263.